Research Square

Preprints are preliminary reports that have not undergone peer review.
They should not be considered conclusive, used to inform clinical practice,
or referenced by the media as validated information.

Enzymatic Simulation by (NAMD), Molecular Docking, Mutation, Structural and Thermodynamic Analysis of Xylanase (Xylcm8) Obtained from Camel Rumen

Marzieh Rajabi
National .Institute of Genetic Engineering and Biotechnology (NIGEB)
Narges Nasrollahi
National .Institute of Genetic Engineering and Biotechnology (NIGEB)
Marjan Rajabi
Tehran University
Kambiz Akbari Noghabi
National .Institute of Genetic Engineering and Biotechnology (NIGEB)
Hossein Shahbani Zahiri (shahbani@nigeb.ac.ir)
National .Institute of Genetic Engineering and Biotechnology (NIGEB)

Research Article

Keywords: Xylanase, Bioinformatics, Enzyme alignment, Nanoscale molecular dynamics (NAMD), Simulation, Molecular docking, Thermodynamics, Structural study

Posted Date: February 28th, 2022

DOI: https://doi.org/10.21203/rs.3.rs-1269403/v1

License: This work is licensed under a Creative Commons Attribution 4.0 International License. Read Full License

Abstract

Xylanase is one of the essential enzymes in divergent industries such as Pulp bleaching, cosmetics, and beverages. It has been widely used in food and pharmaceutical industries and obtained from bacteria, fungi, and crustaceans that is mainly responsible for the hydrolysis of β-1,4 bonds in xylan polysaccharides. Structural and bioinformatics studies of xylanase, can be a contributory and effective aspect of enzyme metabolism and function in polysaccharide components hydrolases. Multiple methods and bioinformatical tools have been used in this study to achieve the whole enzyme structure. The exact enzyme location in the membrane and the main amino acid in the catalytic site have been obtained using computational approaches. This study covers some subjects as enzyme modeling, simulation, structural alignment with similar enzymes, and even docking analysis.

Introduction

Xylanases are member of hydrolases enzymes and can catalyze glycosidic structures [1]. They degrade endo beta 1–4 xylanase bonds between xylopyranosyl residues in their specific polysaccharide, xylan, from non-regenerative ends and make xylooligosaccharide, xylose, xylobiose, etc [2]. Xylanase can be found in bacteria, fungi like *Trichoderma sp*. and *Aspergillus sp*., marine algae, and crustaceans, which fungal and bacterial consist of the main part [3]. As mentioned, they can produce xylooligosaccharides (XOS) in various fields and industries like pharmaceutical, animal feed, and agriculture, even they have prebiotic properties [4]. Most of the xylanases are active in the presence of Cu2+, Mn2+, Fe2+ [1, 5–7]. XylCm8 is active in the presence of heavy elements, Co2 + and Zn2+. Camel's rumen metagenome includes many different species: protozoa, methanogen, fungi, and bacteria, and the last group, bacteria, form the main population of the rumen. *Fibrobacters* and *Neocallimastix patriciarum* are the dominant part of this population [8–11]. In this study, XylCm8 is in GH11(Glycoside Hydrolases 11) family group. The catalytic site has - jelly role structure and has two parallel - strand forms. Their name is A and B with a deep and long cleft; even the active site has two putative catalytic amino acids, glutamate, with catalyst and nucleophilic roles. This family has various substrates, high activity in divergent pH and temperatures, high catalytic power, and small sizes [12–17]. As mentioned, Xylcm8 is in the family 11 groups, and for the first time, we did some bioinformatics study to identify its function and overall structure. In this study, enzymatic predict 3D structure was done by homology modeling techniques [18, 19]. This technique requires reaching accurate quaternary or tertiary structures of the proteins even for reliable free energy prediction [20, 21]. This study determines the correct position and precise interaction between ligand and enzyme receptors. Structural comparison and sequence alignment with the studied enzyme by other similar enzyme was measured, and distinct catalytic amino acid with a similar sequence was identified by accurate position simulation in the membrane. Determining factors that affect catalytic site and enzyme activity by making mutations of some amino acids, enzymatic kinetic parameters and, activity were measured.

According to (Fig. 1), the bacterial membrane structure and the extracellular xylanase enzyme is dedicated. The addition of IPTG (isopropyl β-D-1-thiogalactopyranoside) leads to the induction and expression of xylanase enzyme (Xylcm8) in the *Escherichia coli Bl21* expression strain. In a more detailed view, the bacterial membrane consists of different structural membrane compositions such as pilus, a hair-like structure associated with bacterial adhesion [22]. It plays a vital role in exchanging genetic information and bacterial bindings. In addition, the bacterial outer membrane is an asymmetric bilayer composed mainly of phospholipids, lipopolysaccharides, integral membrane proteins, and lipoproteins. Outer membrane protein A (OmpA), the major component among the outer membrane proteins of gram-negative bacteria such as *E.coli*, is a key virulence factor that mediates a multitude of functions [23]. The position of the xylanase (Xylcm8) enzyme in the outer membrane has been investigated and simulated in the presence or absence of substrates (here, xylotriose) by bioinformatics analysis. The enzyme extends across the bilayer by two beta-strands. If a substrate enters the active site of the enzyme, the formation of an enzyme-substrate complex leads to the enzyme being

placed in the bacterial membrane at an angle of 80 degrees. If the active site no longer binds to the appropriate substrate, the enzyme changes shape, located at a lower angle (about 60 degrees) in the bacterial membrane. The substrate region with the most interaction with the major amino acids in the active site is colored as yellow dots. According to docking studies, the most interaction of the substrate with the amino acids Gln, Glu (which plays an important role as a neurotransmitter), and Tyr. The *helical* form of the enzyme structure is also colored red, and the B-sheet strands are colored purple.

Material And Methods

Sequence alignment and homology modeling

The Basic Local Alignment Search Tool (BLAST) was used to compare nucleotide or protein sequences (https://blast.ncbi.nlm.nih.gov/Blast.cgi). The xylanase-encoding gene (xylcm8) was obtained from a camel rumen metagenome which was available from a previous study by Shahbani Zahiri et al [24]. The sequence data of xylanase enzyme (XylCm8) was submitted in National Center for Biotechnology Information (NCBI) and in the Uropean Nucleotide Archive database (ENA) with nucleotide accession number (KX644155) and amino acid sequence in UniProt database with accession number (A0A1W5YNX4). Sequence comparison proved that this enzyme is related to Glycoside Hydrolase Family 11 (GH11). The enzyme has 1044 nucleotides and 347 amino acids, which has the highest similarity with *Fibrobacters* xylanases in nucleotide sequence with Query Cover, 99%, and identity of 91.53%. The xylanase enzyme's physical and chemical properties as the number of amino acid, molecular weight, positive and negative charge, half-life were measured by online database param prot expasy (https://web.expasy.org/protparam/), 347 amino acids, 37838.13 Da, 37 and 38 amino acids with a negative and positive charge. Enzyme location clarified by PSLpred (https://bio.tools/pslpred). This online server, PSLpred, showed an outer- membrane enzyme in *E.coli*, and it can be secreted slightly outside the membrane [25]. Phylogenetic tree analysis and alignment were performed by using Molecular Evolutionary Genetics Analysis (MEGAX) software [26]. Seven similar sequences were used for alignment. Final sequence alignment was used to create five models by Robetta and RaptorX servers (https://robetta.bakerlab.org/), (http://raptorx.uchicago.edu/). Using Rosetta design server (http://rosettadesign.med.unc.edu/submitjob.php), 2 Ab's were produced to identify model accuracy [27]. The best model with the lowest Discrete Optimized Protein Energy (DOPE) score was selected for more statistical and designing experiments. ProSA web (https://prosa.services.came.sbg.ac.at/prosa.php), PROcheck and Template Modeling Score,Tm score, and Z score were done for quality measurement [28–30]. Ramachandran plot was done by PROcheck online server (http://www.csb.yale.edu/userguides/datamanip/procheck/manual/index.html). The enzyme's secondary and territory structures were measured by online servers: Phyre-2 (http://www.sbg.bio.ic.ac.uk/phyre2/html/page.cgi?id=index) and even by some applications such as Pymol, AzMol and Molegro, Chimera, and ChimeraX. ChimeraX simulated crystallographic model of the enzyme and hydrophobe and hydrophilic interactions between catalytic site amino acid were identified [31]. The homology modeling was done by Swiss model and Scratch proteomics online server (https://swissmodel.expasy.org/qmean/6pqvCC), (http://scratch.proteomics.ics.uci.edu/cgi-bin/new_server/sql_predict.cgi). The signal peptide identification was performed by SignalP-5.0 (https://services.healthtech.dtu.dk/service.php?SignalP-5.0), InterPro (http://www.ebi.ac.uk/interpro/) and PHOBIUS entry (https://phobius.sbc.su.se/). Also, enzyme location and thermodynamic parameters in the membrane were done and calculated by online servers Folding of Membrane-Associated Peptides (FMap), NCBI, Oligocalc, pepdraw, and PSI-blast based secondary structure (PSIpred) online servers (https://membranome.org/fmap), (http://bioinf.cs.ucl.ac.uk/psipred/anduuid),(http://biotools.nubic.northwestern.edu/OligoCalc2.01.), (https://pepdraw.com/), (https://membranome.org/tmdock). Mutation created by ChimeraX. Statistical measurement performed by Design Expert 11 software. Protein simulation conducted by Visual Molecular Dynamics (VMD), ChimeraX softwares and, CharmmGUI (https://www.charmm-gui.org/) online server. At last, RNA analysis was done by RNAFold

and RNA structure prediction of Mathew lab online servers (http://rna.tbi.univie.ac.at//cgibin/RNAWebSuite/RNAfold.cgi?PAGE=3andID=p16y5OBZOA), (https://rna.urmc.rochester.edu). By using TMpred (https://bio.tools/TMPred) and TMHMM (https://services.healthtech.dtu.dk/service.php?TMHMM-2.0) online servers we investigated the enzyme position in simulated transmembrane. In this study, different enzymes PDB code were taken from Research Collaboratory for Structural Bioinformatics (RCSB) (https://www.rcsb.org/).

Ligand preparation

Ligand structure was retrieved from PubChem database with accession number (10201852). The precise and optimized study was done by Molegro software [32, 33]. Cavity structure was then performed and optimized. Ligand and binding sites were performed by COFACTOR and COACH (https://zhanggroup.org/COFACTOR/help.html), (https://zhanggroup.org/COACH/).

Docking study

Ligand docking studies were carried out by Molegro virtual viewer software [34]. Ligand Protein Data Bank (PDB) file was saved as SDF format for docking; the other files were saved as PDB and MVD formats. The girth box was demonstrated and selected large enough to include all the possible poses and residues with all feasible structural cavities in the enzyme construction. The ligand was subjected to 50 docking runs. The top three poses were selected, and from them, one of the best possible poses was saved for further study. Molecular visualization of the docked results was clustered by Molegro, Chimera, and ChimeraX and even by expassy prot param online servers. Also, some probable molecular structures were identified by Iterative Threading ASSEmbly Refinement (I-TASSAR) (https://zhanggroup.org/I-TASSER/) and Robetta servers. The root-mean-square deviation (RMSD) alignment between the studied sequence and the most familiar protein was proposed by SuperPose version 1 webserver (http://superpose.wishartlab.com/) [35]. In this study, all calculated RMSD was done for all atoms involved in alignment, especially in the catalytic site. Protein simulation performed by VMD and ChimeraX softwares. Gibbs free energy (ΔG) of the xylanase, XylCm8, was calculated as follow:

$\Delta G = RT \ln Ki$

$Ki = e^{\Delta G / RT}$

ΔG is the free energy of binding sites (Kcal/mol), R (gas constant) with 1.98 units (cal/mol.K), and T (temperature) is known as 298.15 kelvin [36].

Results And Discussion

Modeling of the enzyme is demonstrated as follow (Fig. 2). It was done by Swiss Model and Scratch proteomics database. The local quality score is shown from low quality 0, with red color to high quality 1, in blue. Most of the - strand structures are located as high quality and conserved. The signal peptide part is conserved as low confidence with 28% probability, and the section which is located in the membrane is measured as high confidence part with up to 88% accuracy. The high reliability of signal peptide was confirmed by using the online servers as InterPro, SignalP and, PHOBIUS entry. The Qmean distance constraints (QMEANDisCo), the average per residue score, and the provided error estimate are about 0.55 ± 0.05.

As homology modeling was demonstrated and checked in (Fig. 2), the enzyme alignment was provided by Geneious Prime and JalView softwares. In (Fig. 3), the physicochemical features of the enzyme are demonstrated. The hydrophobicity is different between 0–1; low hydrophobicity (in blue) to high (red line) was shown. In residue 1–21, the

signal peptide part, the hydrophobicity is variable between 0.74–0.62, and among two positions 120 and 135, the region located in the membrane, Ile, the hydrophobicity changes around 0.94, which is predictable.

The total Isoelectric Point (PI) of the XylCm8 is about 7.63, which is neutral, and the total amino acid charge is 44.6%, which is almost lower than the neutral form and is about 5.4% negative (Fig. 3).

Alignment was accomplished between 7 similar enzymes in different specious (Bacterial and Fungal) with Blosum62 matrix (Fig. 4). These enzymes with different PDB codes as 7DMN,6ZA2, 3WP6, 2DCJ, 7MGU, 3B5L, and 2VUL are extracted from the Research Collaboratory for Structural Bioinformatics (RCSB). Mean pairwise identity is around 0-100%, green color shows 100%, green-brown between 30–100%, and red part has lower than 30% identity. Black parts show the confidence of amino acids in various enzymes. Position 251, Ala, 62 Ser, in column are the same in all the studies familiar xylanases. Column 509 and 574, Tyr and the other one, 870, Glu are identical in XylCm8 and the most familiar xylanase enzyme with PDB code 3WP6 from *Neocallimastix patriciarum* (GenBank accession number AF123252) with pair identity between 30–100%. Positions 57,78 ,103,115,141,145,175,211 and 260 have high consensus identity.

According to (Fig. 5), XylCm8 has negative charge amino acids and is considered negative charged. It has Asp, Gln, Glu, and Cys amino acids. Cause of the existing lots of Glu in its structure, this enzyme can be active in acidic buffers as citrate buffer. As we mentioned, XylCm8 has negative charge amino acids though 3WP6, the most similar enzyme (especially in its catalytic site) is considered as a positive charge. 2DCJ, the second enzyme similar to the studied structure, like XylCm8 is negative charge amino acid. All the enzymes in alignment are positive charge amino acids. Proline, negative, and aromatic amino acids (non-polar, polar, and hydrophilic as Tyr, Trp, and Phe) are demonstrated in their structure. Many of the non-polar amino acids such as Ser, Thr, Gly, and Ala are in XylCm8 structure, and because of having Gly in the structure, it can be used as a preservative or dietary supplements in the food industry to solve the anemia suffering and hemoglobin derivative.

According to the result of the Phyre2 server, the second structure of the enzyme is composed of 11% alpha-helix (purple), 46% beta structure (is in pink color), and 23% is in form of coil (blue) (Fig. 6). 34% of this structure is unidentified. It is predicted that the enzyme has two domains and amino acid 238; Glu is determined as a boundary between two parts. Error-values of the XylCm8 structure is measured by ERRAT2 program. It calculated the error value below the 95% rejection limit. The lower resolutions (2-3A˚), their overall quality factor is demonstrated by 91% and the quality factor of the enzyme is 54.167%. Ramachandran plot adjusted by PROcheck online server indicates that most of the residue in the enzyme structure is in - sheet form. The parts that amino acid shouldn't be there, are about 1.3% with 90˚, 135˚ phi, and − 180˚ psi angles. The residues in the additionally and generously allowed region are 10.9% and 2%. The percentage of residue in the most favored region is 85.9%, and it shows the model has acceptable quality in protein fold; according to predictable structure, the results indicate that we have a proper model for molecular docking [37, 38].

The average energy of the enzyme sequence is around 0 (-0.5 - +0.5), and it shows that the enzyme is stable in normal conditions, and the Z.score of the studied model is -3,81. Z score technically indicates how many standard deviations is below or above the population mean; In another word, it demonstrates the total model quality, and it is a beneficial way to point and compare the accuracy of the energy of the structural model from the initial form [39]. XylCm8 Z score is valid and acceptable, and the data is probable to the real structure.

TM score is a metric assessing structural, geometrical similarity between 2 protein models to solve a traditional metric bug in measuring RMSD. It has a value of 0–1, where 1 illustrates a perfect match between the two models. Scores below 0.17 correspond to unrelated proteins, whereas scores higher than 0.5 generally indicate the same fold of proteins in hierarchical domain classification systems, SCOP/CATH [40, 41]. This study compared five simulated XylCm8 models

by I-TASSER and Robetta online servers. The best TM score among them was around 0.58 ± 0.14, the selected model measured by the Swiss Model database. It indicates that the proper and reliable model is selected for this study.

According to the results of Robetta server, the best model with a proper TM score is the first one with a low error estimate (Fig. 7). The membrane part of the enzyme has different error estimates from 1.2–0.98 A˚ [42, 43]. We compared the TM scores between studied xylanase, XylCm8 with 347 amino acids, and the most similar enzyme structure chain A, 3WP6 with 228 amino acids. TM score was indicated 0.1558 among 225 residues in common. RMSD of the common residue demonstrated as 20.687. Superposition of the TM score, lower than 5 A˚, has been reported 22 with RMSD 3.57.

Five different poses were detected in the enzyme, XylCm8. There are five cavities in the structure. The active site of the enzyme was identified, and the docking program was generated in disparate locations. The best location with the lowest Molecular Docking (MolDock) score was selected. The docking program was done with ten runs. The best MolDock score (GRID) was − 120.932. These five poses are indicated in (Table. 1), remarkably. The RMSD of the XylCm8 in comparison with the most identical enzyme, 3WP6, was considered, and the result was noticed in (Table. 3).

Table 1
MolDock chart and scores of XylCm8 with five different poses.

Different Poses of Ligand for Docking	MolDock Score (GRID)	MolDock Score	Rerank Score	Torsions
1	-120.932	-85.7833	-80.8915	4
2	-118.613	-91.3556	-42.0097	4
3	-117.247	-92.7537	-45.085	4
4	-116.937	-107.852	-100.225	4
5	-115.389	-97.1327	-79.7879	4

Best MolDock score (GRID) and MolDock with − 120.932 and − 85.8915 is selected, and docking was accomplished (Table. 1).

Table 2
Ligand poses and scores for docking.

Ligand Poses	MolDock Score	Rerank Score	HBond
1	-95.3145	-54.6823	-13.1162
2	-92.632	-84.0667	-17.0092
3	-83.5427	-52.0072	-12.8954

Five Ligand poses were detected. Three best poses were selected, and the MolDock scores were identified. The first pose was the best one, with a score of -95.3145. This negative score relies on better stability and refining in the docking. The ligand was fit in the receptor part without water molecules and any hydrogen bond (Table. 2).

RMSD was calculated in this study. root mean square deviation (RMSD) can make a reliable comparison between two macromolecule models for evaluating and proposing the best docking location between them, and it demonstrates the best energy pose, as it identifies the lowest one, in designing and molecular modeling [44, 45]. The RMSD of the studied enzyme was compared to the highlighted, most similar enzyme, 3WP6, and the results were calculated (Table. 3). The estimated raw RMSD of the XylCm8 is 8.9 ± 4.6 A˚. It is predicted that the enzyme has two active sites, and its structure contains: E 132 and E 230. The results are calculated and analyzed by Superpose Wishartlab online server.

Table 3
Structural alignment to gide the RMSD superpose.

Local RMSD						
	α Carbons	Backbone	Heavy	All	Structure	Residues
RMSD	16.29	16.18	16.33	16.33	XylCm8	1–24,25–37,38–86
Atom	86	344	440	440	3WP6-Chain A	22–45,47–59,61–109
Global RMSD						
	α Carbons	Backbone	Heavy	All	Structure	Residues
RMSD	28.26	28.21	27.96	27.96	XylCm8	20–21,22–45,47–59,61–149,152–153,156–183,185–237,239–254
Atom	227	908	1597	1597	3WP6-Chain A	1–24,25–37,38–126,127–128,129–156,157–209,210–225

Table 4
Custom alignment to gide RMSD superpose.

Local RMSD						
	α Carbons	Backbone	Heavy	All	Structure	Residues
RMSD	3.49	3.60	4.69	4.69	XylCm8	118–139
Atom	22	88	122	122	3WP6-Chain A	94–115
Global RMSD						
	α Carbons	Backbone	Heavy	All	Structure	Residues
RMSD	3.49	3.60	4.69	4.69	XylCm8	118–139
Atom	22	88	122	122	3WP6-Chain A	94–115

The indicated RMSD for the whole molecule is 8.9 ± 4.6 A˚ while comparing XylCm8 with 3WP6-Chain A highlights the structural and custom ones. Structural one shows a considerable variation and different atoms between both models; the RMSD of this comparison is so high, and it covers a wide range (Table. 3). Hence, it dedicates more than the main number, which was presented at first, about 8.9, and structural form can't be reliable. However, the customs form of RMSD covers a short range of atoms with a lower number than the initial form. It can be more accurate and reliable because it indicates the stable position of the molecule and demonstrates the permanent energy level (Table. 4). α carbons RMSD is 3.49 between 22 atoms and dedicated 3.6 in the backbone of both structures through 88 atoms. These numbers in global and local custom RMSD are the same by superposing. Overall, RMSD for both models in the local and global custom alignment is 4.69 among 122 atoms. The deduction of the custom alignment RMSD measurement demonstrates that residue 118–139 shows the number 4.69 in RMSD calculation, which is suitable and desirable. This selected part of the enzyme is located in the membrane and should have lower energy to be stable through all incidence mutations. In addition, this highlighted part in the membrane is a component portion of the catalytic site of XylCm8. Residue 94–115 in 3WP6 illustrate the overall RMSD, respectively.

From amino acids, 120 to 135 (between two Ile) are located in the bacterial membrane. This part of the amino acids acts as an anchor. It has 16 amino acids (full of Gly, Trp, Ile, aliphatic and hydrophobic amino acids, and Glu, an acidic

amino acid). It anchors inside the membrane (Fig. 8). This part is located in the loop and - strand structures. The hydrophobicity of this part is + 8.99 kcal/mol with an extinction coefficient of 13980 $\mathrm{M}^{-1}.\mathrm{Cm}^{-1}$, pI = 4.09, and net charge − 1.

To compare the Gibbs Free Energy (ΔG) of the XylCm8 native form with the mutated one and investigate the affection of this substitution on the stability of the enzyme, some mutations are manufactured in the membrane section of the enzyme. These mutations are in disparate parts: Lue130, V131, and Lue-V as a unique part.

Table 5
Thermodynamic Constance in native form and three various mutations by OligoCalc 2.01 online server.

Name	R.lnK (cal/˚K. mol)	ΔG (Kcal/mol)	ΔH (Kcal/mol)	ΔS (cal/˚K. mol)
XylCm8 (Native Form)	33.404	1702.7	9098.4	23828.3
Lue130 → Arg	33.404	1780.3	9240.7	24036.4
V131 → Arg	33.404	1780.5	9237.5	24025.3
Lue130,V131 → Arg	33.404	1782.2	9245.4	24045.3

For measuring the stability of the enzyme in the membrane and make it more soluble in the water for easier purification, the mutation in three sections was conducted: Ile 130, V 131, Ile130-V131 (3 membrane amino acids in the - strand part), and were replaced with a positive, hydrophilic amino acid Arg (Table. 5). All the consequences are measured at 25˚ with 1M NaCl at pH = 7. The results are demonstrated in (Table. 5). ΔG of the native form of the enzyme is 1702.7 Kcal/mol, and its entropy ΔS is 23828.3. The best substitution of the amino acids is in mutation with V 131; as in both mutations,130 and 131, the free energy almost is equal, it's about 1780.3 Kcal/mol among other mutations, and it makes the enzyme more stable but the entropy of the mutated 131 is lower than 130 its described as 24025.3 (cal/k.mol). Gibbs free energy (ΔG) is an unit that clarifies the stability of the reaction; the lower amount of ΔG, the better stability, and eventually in docking analyses the better matching with ligand [46, 47]. Gibbs free energy illustrates the reaction is spontaneous or not and in a simultaneous reaction with entropy (ΔS) [48, 49]. Substitution with both changes in both sections in the membrane, Ile130, V131, has the most authority in thermodynamic constants, ΔG and ΔS. It shows that this mutation changes ΔG up to more than 80 numbers. Hence, this substitution makes entropy so high, 24045.3 cal/K.mol, and it changes and makes the enzyme's structure more unstable. It would be better for the enzyme to be soluble in water but negatively effects on its molecular structure. Among these three mutations, the double mutation has the most impact on the ΔG and ΔS, though single mutation on a unique part of the molecule structure makes no changes on ΔG, it is about 1780 Kcal/mol and changes ΔS from the native and raw form to 24025 ± 11 cal/K.mol. From these mutations, the one, which engendered V131 to Arg is selected as the best substitution from these three mutations, cause its ΔS to be 24025.3 cal/K.mol with its free energy ΔG of about 1780.5 and is indicated as a stable form of the enzyme.

As indicated in (Fig. 9), some intra interactions can be detected in the mutated form. The enzyme would be more positive and hydrophilic by replacing R instead of Lue and V. Both Arg in mutated parts have a distance of about 2.399 A˚ from each other; Arg 131 has a space of approximately 2.989 A˚ from Thr 126. The replacement angles of the Arg in position Lue130: φ -87.3, ψ 113 and ω179 and for V130 is: φ -140, ψ 145 and ω 178. Mutated Lue is surrounded by some amino acids such as Lys 188 (1.520 A˚), Phe 187 (1.530 A˚), Lys 185 (1.530 A˚), Pro 129 (1.547 A˚). This mutation caused the head of the loop part to bend inside the enzyme. The rotamers, which played an essential role in making mutation form in the enzyme, were demonstrated and selected; for choosing Arg in replacement of V131 and even in Lue130, with 0.12% and 0.1% prevalence was detected.

Analysis of Gibbs free energy (ΔG) was done with Response Surface Methodology (RSM) by Design Expert 11, with 13 runs (Fig. 10). The best model was selected with the sum of square 10533.75, mean square 2106.75, F-value = 2, which implies the model isn't significant relative to the noise and the percentage of the noise is 36.61%; and with P-value 0.3661. In addition, the coefficient estimate is 1742.45. It is better by making interactions and analyzing the substitution in other residues to check the best reliability in future studies. The adjusted $R^2$is 0.4167, and the predicted $R^2$is -2. As predicted, the best free energy is 1780 kcal/mol by the result; in this range, the molecule must be more stable. In both surface response pictures, the range of Gibbs free energy from low to high is dedicated in (color blue) 1702.7 to (red) 1782.2. At left, (Fig. 10a), is the predicted model at the best and most accurate situation, and the model (Fig. 10b) presented at right illustrates the desirable model. Pink colors show the design points below the predicted value, and the red ones show the points above the predicted value. The desirable predicted value: ΔH = 9098.4, ΔS = 24045.3 and ΔG = 1715.95.

As α helix form can play a delighted role in enzyme stability, the presumption of α helix creation was examined in the membrane, and the results are as follow [50]. The most effective part for selecting the best form of α helix is the end of each section (Table. 6).

Table 6
Thermodynamic measurement of mutated residues in α helices form of the section in the membrane by membranome server. Some features as binding energy, angle and stability in water are compared with the enzyme model Xylcm8.

Name	Segment	Sequence	Stability Relative to Coil in Water kcal/mol	Stability Relative to Bound Coil kcal/mol	ΔG Transfer, kcal/mol	Tilt angle, °	Depth/thickness, Å	Binding Energy, kcal/mol
Arg130	2–5	GIYG	-0.0	0.4	-4.8	87	4.8	-3.9
	10–13	PRVE	0.2	0.3	-3.3	70	1.4	
Arg131	2–5	GIYG	-0.0	0.4	-4.8	87	4.8	-5
	10–13	PLRE	-1.1	-0.6	-4.3	81	1.6	
Arg130,131	2–5	GIYG	-0.0	0.4	-4.8	87	4.8	-3.9
	10–13	PRRE	0.2	0.2	-3	77	1.4	
Native	2–5	GIYG	-0.0	0.4	-4.8	87	4.8	-4.2
Form	11–13	LVE	-0.3	0.3	-3.8	71	3.9	

As demonstrated in (Table. 5), the most effective substitution is in location 131 by replacing V131 with Arg. The binding energy of this replacement is in the lower form among the others, even the native structure, -5, which illustrates that the enzyme will be more stable by this replacement (Table. 6). Even transfer ΔG is sufficing in its minimized form, -4.3.

According to (Fig. 11), as we supposed the same enzyme interactions between two membranes, the outer membrane is in red color and the inner membrane considered in blue color. The predicted α helix form of the enzyme is determined with three divergent mutations and native forms. The interactions between XylCm8 and membrane are illustrated in green color. Positions are as follows: (Fig. 11a) with double mutation, (Fig. 11b) native form of XylCm8, (Fig. 11c) mutation in position 131, V, (Fig. 11d) by changing the position 130, Lue. As demonstrated at first best substitution is known in (Fig. 11c). As it was mentioned, the transmembrane form of the XylCm8 was investigated by TMpred and TMHMM online servers. It clarified that the enzyme isn’t detected in the transmembrane part, and it determined that

XylCm8 is more hydrophilic. By simulating the enzyme in transmembrane, among 347 amino acids, only one site between 50 amino acids is analyzed as a hydrophobic part.

In addition, for detecting the probability of the existence and function of the small interfering RNA (siRNA), we analyzed and designed the enzyme's secondary structure and predicted and specified the thermodynamic measurement and activity in the cell by RNA Structure Mathews Lab and RNAfold online web servers. Even for predicting and analyzing mRNA and miRNA and their function in protein translation or in designing RNA vaccines in the clinical stage and for cancer therapy as gastric cancer, in further study, we can combine these findings and benefit from these approaches [51].

Prediction of the lowest free energy structure and a set of low free energy for a sequence are based on the conclusion of two predicting RNA structure methods as RNA structure fold. The second one is based on RNA structure MaxExpect results (https://rna.urmc.rochester.edu/RNAstructureWeb/Servers/MaxExpect/MaxExpect.html), in RNA structure web server, Rochester Lab as it mentioned, which generate highly probable base pairs structures. This alternative structure prediction method may have higher fidelity in structure prediction (Fig. 12). These figures have more than ≥ 99% probability. The minimum free energy prediction of the secondary structure is about − 335.80 kcal/mol, and the free energy of the thermodynamic ensemble is about − 355.34 kcal/mol. The entropy range in (Fig. 12a) is different from the lowest to a high number, 0–2.9, minimum with red color and maximum in blue. The tail of RNA is in the middle to high range of entropy. Some parts are demonstrated in mini loop forms as the red is in the stable form stage. Others show the bending forms of RNA in reactions and interactions of intracellular mechanisms. Form (Fig. 12b) and (Fig. 12d) colored by position; in this type of color, nucleotides canvas according to their position in the molecule. Lower numbered nucleotides are closer to the 5' end and are colored green. Nucleotides in the middle are colored yellow, whereas nucleotides near the 3' end are colored red. Form (Fig. 12d) shows the fully bent position of the RNA in the reaction. Form (Fig. 12c) colored by sequence according to the nucleotide types. Each color illustrates a sign: yellow (adenine), green (cytosine), blue (uridine), and red (guanine). Commonly, form (Fig. 12c) is populated by G and U nucleotides, and branched areas in (Fig. 12b) and (Fig. 12d) are closer to 5' end string-like area are more comparable to 3' end. Generally, the 3' end can play an essential role in interactions and molecular communications.

Enzyme simulation was done by Nanoscale Molecular Dynamics (NAMD) software with VMD, ChimeraX software's, and CharmmGUI online server (Fig. 13). CharmmGUI performed the building of the bilayer membrane with 0.3 M NaCl, which was the main NaCl concentration in the lysis buffer. Total lipid in the upper leaflet is about 13418.1, and in the lower leaflet is 12071.4 that's because of phosphatidylglycerol (POPe) and sphingomyelin (PSm). Posing the enzyme in the membrane has been adjusted by VMD. It dedicated the part of - strand structure to the membrane, which plays a role in the docking process. It demonstrated that the hydrophobic section composed of 16 amino acids is located in the outer membrane of XylCm8 with some hydrophobic interactions. We compared structural simulation of both hallmark enzymes, XylCm8 and 3WP6. XylCm8 is an outer membrane, as mentioned initially, though 3WP6 would be expressed out of the cell and isn't located in the membrane. Still, to illustrate its simulated interaction with the membrane, we added some ceramides (CER) and glycolipids bonds to show the hypothetical shape of its connection to the membrane. As shown in shapes (Fig. 13f, g, and h), XylCm8 isn't a transmembrane enzyme, and some of its catalytic sites are surrounded by the outer membrane of *E.coli*. Both enzymes have the same catalytic sites, a hole-shaped form surrounded by six -Sheet layers, demonstrated and well-known description as an especial sign for glycoside hydrolase family 11 (GH11).

Table 7
Ligands and binding sites in XylCm8.

Rank	C-score	Cluster Size	PDB Hit	Ligand Name	Ligand Binding site Residue
1	0.38	64	1c5iA	DF Xylopyranose	50,80.82,123,125,132,134,175,179,187,189,230
2	0.16	27	3wp6A	-D xylobiopyranose	52,54,82,84,123,125,179,180,181
3	0.10	18	4hkwA	Xylopyranose	80,119,134,179,175,189,191,230,232
4	0.03	6	2VGDA	Xylobiose and xyloteriose	80,116,117,119,134,142,148,150,151,153,175,189,230
5	0.01	2	3wp6A	Xylopyranose	116,117,148,234

In (Table.7), 5 different ligands and their binding sites have been mentioned. This analysis was performed by COFACTOR and COACH based on the I-TASSER prediction server. Best ligands are identified as 1,2-Deoxy-2-fluoro-xylopyranose with C-score 0.38. Checkerboard score (C-score) is the confidence score for prediction. C-score ranges (0–1), where a higher score indicates a more reliable prediction [52, 53]. This study and enzyme analysis was performed by xylan, and it is composed of - Xylopyranose chain. As illustrated, most amino acids in the catalytic site are Arg 175, Gln 189, Trp 125, Glu 132, Asp 80, and Ser 179.

Positive and negative charge amino acids significantly influence the structure and protein folding. It has been reported that positively charged amino acids can change the target molecule and make it a hyperpolarized one, and this substitution can have a considerable effect on the toxicity of the macromolecule [54]. The studied enzyme is almost a bit negative charge. Also, hydrostatic pressure can have a negative and positive effect on the thermodynamic section of the protein and can change folded and unfolded proteins and make them more stable or vice versa [55]. Some intra forces between encoded and coded atoms in macromolecules as proteins can affect their stability in divergent thermodynamic situations. α helices can make the protein structure, fold or unfold, more stable in different conditions such as vigorous temperatures and it can provide a better protein contribution. In some cases, by protein designing modeling, it had been revealed that protein could be stable without disulfide or metal coordination. Some designed proteins can act as an inhibitor for various intracellular interactions [56]. Even the electrostatic strength can significantly affect protein forms and contributions and makes protein funnel in modeling. Also, by using this approach, Debye-Huckel potentials, approximating the potential of mean force (PMF) between ions by the average electrostatic potential, and measuring associate interaction and water, structure, and energy model (AWSEM), we can analyze the electrostatic forces between macromolecules [57]. We separately analyzed some features that can affect electrostatic as associate interactions and structure and energy of substitution model, and we focused on the structural model and intra molecular interactions. In this study, by making and improving single point mutations (SPMs) and by measuring multiple computational structural modeling even in empirical conditions and study, the effect of some mutation on catalytic site pinpointed [58]. In some cases, it's observed that the electron-withdrawing of some parts of the anionic (negative sections) of the amino acid in peptide binding can reduce the negative charge of the molecule by reducing the negative charge of the amino group and making it more soluble, even by activating the carboxylate end of the amino acid it can interact with CO2 molecule [59]. So far, according to assumptions, the charge of amino acid propagation is related, merely for the whole structure of amino acid not for the chain of them, and the chain is remained voided [60]. Hydrophobicity is a crucial feature in protein modeling and function, and in some cases, by using some in-vitro techniques as HILIC (Hydrophilic Interaction Liquid Chromatography for analyzing hydrophobicity of the proteins) and RPLC (Reverse Phase Liquid Chromatography for analyzing proteins and amino acids), the hydrophobicity and

hydrophilicity of the protein can be detected [61]. This highlighted feature (hydrophobicity) engenders when a non-polar amino acid angel is about θ 90, and switch to hydrophilic form as 90 θ and by θ = 0, it's equally neutral [62]. The part located in the lipid bilayer usually has an angle of about 90˚ or a bit less but more often, it can be more than that, and by replacing polar amino acid substitution; it changes strikingly to be more hydrophilic. The solvent concentration has a hallmark influence on protein folding and hydrophobicity, preventing protein misfolding. The right choice of solvent concentration can hamper protein aggregation and the best solvent for making and adjusting a proper hydrophobicity is water; even nonpolar concave protein surfaces are more hydrophobic, and in contrast, hydroxyl groups can decrease the hydrophobicity [63–65]. We performed the enzymatic assay in water with 0.3 M NaCl for protein expression. Moreover, mutated proteins have the same number of polar and non-polar sides, but in contrast, geometrical arrangement and their influence are on strong interaction with water. So we expect this assumption that our mutation forms conflict with each other in various strength interactions with water [65]. It has been reported that oil-water in normalized concentration can affect the charge of protein, stability, and hydrophobicity of it, and it can change the protein absorption process lesson or decline [66]. We experimented with water without an oil environment, and it's plausible that XylCm8 can act more freely and functionally with its specific substrate, xylan. Maybe the absorption process would be better and easier when it's soluble in water. Cofactors can affect membrane permeability and make the enzyme function and structure more hydrophilic, though no special cofactors are detected in this study, as we mentioned, heavy elements like Co2 + and Zn2 + can play an important role in some cases, as cofactor on Xylcm8 activity [67]. The other feature, which is a hallmark in protein folding study, is the hydrogen bond and its effect on the interactions between ligand through docking. A hydrogen bond is an electrostatic one, and it plays an essential role in water and ligand intermolecular interactions; ligand is somehow static in hydrogen intermolecular interactions [68]. H-bond can decrease the interactions between ligand and acceptor by creating water bulk. These weaker and stronger bonds make this intra interaction (ligand-acceptor) more unstable, and as a result, the s-s and w-w H-bonds, some examples of H-bonds among various atoms as the oxygen-nitrogen interplay, make more affinity in ligand-enzyme interactions by reducing the entropy; and precisely, this water bulk changes and lowers the interactions between XylCm8 and the specific substrate, xylan [69]. Some parts of the hydrogen bond act as an acceptor and others as a donor. The strength between acceptor and receptor is fundamental; even the angels in these interactions are so substantial. The CHI-energy function is so crucial in reliable docking performance. Chi-coeff with equal 1 represents the accuracy of the protein folding and binding; and with coeff = 2, it dedicates a low accuracy in protein folding [70]. As it represented, the bonding angles between acceptor and receptor or ligand and protein are so momentous. The ligand-protein angles in this study are about: 0.68, 1.35, 3.24, 3.18, and 1 A˚ in different residues in vigorous positions. As it reported, one of the significant ligand-acceptor interactions is the hydrophobic one. In this study hydrophobic bond section of the XylCm8 have a significant role and it made the enzyme more stable in the membrane; as mentioned, we couldn’t identify any special coenzyme for XylCm8; and the main and specific ligand for the studied enzyme (Xylcm8) is xylan, especially some mono forms of it such as xyloteriose and xylobiose; hence, it's reported that vitamin C can be pointed as a cofactor for xylanase in some fermentation processes [71]. Since XylCm8 has the most similarity with 3WP6, the structural RMSD has been measured on both enzymes, with global and local RMSD 4.69 in a range of different numbers of residues, in 118–139 residue enzyme parts (Table. 3). The main amino acids in docking demonstrated as Glu(132,230)-Tyr(134,176,119)-Gln189, and while it's been reported in structural alignment with 3WP6, Trp(125,102,32)-Val206-Gln161- Arg148 and Asp57 and it shows the most variability and range of amino acids in this situation (Fig. 6b). In both dockings, Glu plays the prominent role as the main amino acid in the active site, and that was completely predictable while it's known as the principal amino acid in the GH11 family active site, as we mentioned [17, 72]. We made some mutations to make more hydrophilicity and created the novel enzyme form that acts freely from the membrane. Most of the enzymatic mutations, especially on the xylanase GH11 family are produced to change the catalytic site and make the more active forms of the enzyme to degrade the substrates as xylobiose and xyloteriose [73, 74]. In this study, the best and appropriate substitution is in position Val131 with Gibbs free energy ΔG = 1780.5 (kcal/mol) and ΔS = 24025.3

(cal/˚K.mol) (Table. 5). More substitutions (by increasing and decreasing hydrophobicity) in divergent catalytic sites are suggested.

Molecular docking and simulation have been accomplished in different dimensions and poses with disparate bioinformatics software for demonstrating highlighted detailed measurement between the interaction of enzyme and ligand. These mutations were carried out for measurement of enzymatic behavior and even for checking energy level and enzymatic stability (investigation of thermodynamic properties) in different conditions. XylCm8 with about 65% per identity with 3WP6 has the most structural analogous, strikingly, in the catalytic site. For this well-known reason, simulation has been performed to examine the structure of the enzyme in particular interactions measurement and enzymatic catalytic site similarity with 3WP6. Generally, the mutations created, although the best of them are highlighted as in point residue 131 (Table. 5), most of them make the enzyme form in different degrees more unstable.

Conclusion

In conclusion, this is the first bioinformatics study in the scope of communicational, simulation, and homology modeling and thermodynamics features of XylCm8, which was obtained from camel rumen and manufactured in a detailed and stringent. Ramachandran results indicate that most residues are in the favorable and authorized zone. Molecular docking, predicting ligand poses and structural enzymatic alignment and interactions performed by various bioinformatics methods and softwares strikingly. By making some mutations in the hydrophilic site of the enzyme, we displayed that we can have high enzyme activity with low stability for designing and making different enzyme models in further studies. Even by enzymatic simulation with NAMD and some bioinformatics software's as VMD, we pointed the right position and interaction of the enzyme in the membrane. Identifying the results of RMSD alignment, mRNA synthesis, divergent mutations emphasizing the suitable enzyme poses in the outer membrane can support researchers in designing a beneficial method in clinical drug designing as in live vaccine. Fortunately, the result of this study will coordinate us in comprehension figuring out the molecular interactions and thermodynamic conception in further studies. Moreover, additional detailed electrostatic measurement and inhibitors' influence on enzymatic function is suggested to be examined.

Declarations

Data availability

The raw and processed DNA-sequence data, which is generated and used to support the findings in this study, has been deposited in the European Nucleotide Archive database (ENA) under the accession number (KX644155). The protein sequence, which is generated in this study, has been deposited in the UniProt and ENA database under the accession number (A0A1W5YNX4). The macromolecular structure data, as NMR and chemical shifts, in this study have been deposited in the Biological Magnetic Resonance Data Bank (BMRB) under the accession and entry number (51279). Even another macromolecular structure study on the other experimental method as X-Ray diffraction has been deposited in the Worldwide Protein Data Bank (wwPDB) under the accession number (D-1300027489).

The Ligand structure data used in this study is publically available in the PubChem database under the accession number (10201852) (https://pubchem.ncbi.nlm.nih.gov/compound/Xylotriose).

The enzyme, which has the most similar structure to the Xylcm8, is publically available in the GenBank database under the accession number (AF123252).

Acknowledgements

We thank all the writers from National Institute of Genetic Engineering and Biotechnology (NIGEB) and Tehran university, who helped us for preparing this article.

Author contributions

M.R.[1,2] designed the (Fig. 1) and prepared bioinformatics analysis. H.S.Z. and K.A.N. developed the main idea, initiating the project. M.R.,N.N.,M.R. wrote the main manuscript text and revised the article. H.S.Z. and K.A.N. designed and supervised the research. All authors reviewed the manuscript.

Competing interests

The authors declare no competing interests.

References

1. Zarafeta, D., et al., *XynDZ5: a new thermostable GH10 xylanase*. Frontiers in microbiology, 2020. **11**: p. 545.
2. Chen, Z., et al., *Purification and characterization of a new xylanase with excellent stability from Aspergillus flavus and its application in hydrolyzing pretreated corncobs*. Protein expression and purification, 2019. **154**: p. 91–97.
3. Burlacu, A., C.P. Cornea, and F. Israel-Roming, *Microbial xylanase: a review*. Scientific Bulletin. Series F. Biotechnologies, 2016. **20**: p. 335–342.
4. Brandt, S.C., et al., *Aspergillus sydowii: Genome analysis and characterization of two heterologous expressed, non-redundant xylanases*. Frontiers in microbiology, 2020. **11**.
5. Bhardwaj, N., et al., *Cloning, expression and characterization of a thermo-alkali-stable xylanase from Aspergillus oryzae LC1 in Escherichia coli BL21 (DE3)*. Protein expression and purification, 2020. **168**: p. 105551.
6. Katsimpouras, C., et al., *A novel fungal GH30 xylanase with xylobiohydrolase auxiliary activity*. Biotechnology for biofuels, 2019. **12**(1): p. 120.
7. Ping, L., et al., *Production and characterization of a novel acidophilic and thermostable xylanase from Thermoascus aurantiacu*. International journal of biological macromolecules, 2018. **109**: p. 1270–1279.
8. Hinsu, A.T., et al., *Characterizing rumen microbiota and CAZyme profile of Indian dromedary camel (Camelus dromedarius) in response to different roughages*. Scientific reports, 2021. **11**(1): p. 1–14.
9. Kumar, A., et al., *Immobilization of xylanase using a protein-inorganic hybrid system*. Journal of microbiology and biotechnology, 2018. **28**(4): p. 638–644.
10. Rabee, A.E., R. Forster, and E.A. Sabra, *Lignocelluloytic activities and composition of bacterial community in the camel rumen*. AIMS microbiology, 2021. **7**(3): p. 354.
11. Srivastava, S., et al., *Unraveling the camel rumen microbiome through metaculturomics approach for agriculture waste hydrolytic potential*. Archives of Microbiology, 2021. **203**(1): p. 107–123.
12. Bu, Y., et al., *Engineering improved thermostability of the GH11 xylanase from Neocallimastix patriciarum via computational library design*. Applied microbiology and biotechnology, 2018. **102**(8): p. 3675–3685.
13. Cheng, Y.-S., et al., *Structural analysis of a glycoside hydrolase family 11 xylanase from Neocallimastix patriciarum: insights into the molecular basis of a thermophilic enzyme*. Journal of Biological Chemistry, 2014. **289**(16): p. 11020–11028.
14. Karlsson, E.N., et al., *Endo-xylanases as tools for production of substituted xylooligosaccharides with prebiotic properties*. Applied microbiology and biotechnology, 2018. **102**(21): p. 9081–9088.
15. Marasinghe, S.D., et al., *Characterization of glycoside hydrolase family 11 xylanase from Streptomyces sp. strain J103; its synergetic effect with acetyl xylan esterase and enhancement of enzymatic hydrolysis of lignocellulosic*

biomass. Microbial Cell Factories, 2021. **20**(1): p. 1–14.

16. Walia, A., et al., *Microbial xylanases and their industrial application in pulp and paper biobleaching: a review*. 3 Biotech, 2017. **7**(1): p. 11.
17. Wu, X., et al., *Insights into the role of exposed surface charged residues in the alkali-tolerance of GH11 xylanase*. Frontiers in microbiology, 2020. **11**: p. 872.
18. Studer, G., et al., *ProMod3—A versatile homology modelling toolbox*. PLoS computational biology, 2021. **17**(1): p. e1008667.
19. Tseliou, V., et al., *Generation of amine dehydrogenases with increased catalytic performance and substrate scope from ε-deaminating L-Lysine dehydrogenase*. Nature communications, 2019. **10**(1): p. 1–11.
20. Park, H., et al., *Protein homology model refinement by large-scale energy optimization.* Proceedings of the National Academy of Sciences, 2018. **115**(12): p. 3054–3059.
21. Waterhouse, A., et al., *SWISS-MODEL: homology modelling of protein structures and complexes*. Nucleic acids research, 2018. **46**(W1): p. W296-W303.
22. Alonso-Caballero, A., et al., *Mechanical architecture and folding of E. coli type 1 pilus domains*. Nature communications, 2018. **9**(1): p. 1–11.
23. Nielsen, D.W., et al., *Outer membrane protein A (OmpA) of extraintestinal pathogenic Escherichia coli*. BMC research notes, 2020. **13**(1): p. 1–7.
24. Gharechahi, J., et al., *In-depth diversity analysis of the bacterial community resident in the camel rumen*. Systematic and applied microbiology, 2015. **38**(1): p. 67–76.
25. Hoda, A., M. Tafaj, and E. Sallaku, *In silico Structural, Functional and Phylogenetic Analyses of cellulase from Ruminococcus albus*. Journal of Genetic Engineering and Biotechnology, 2021. **19**(1): p. 1–15.
26. Adams, E.M., et al., *Local Mutations Can Serve as a Game Changer for Global Protein Solvent Interaction*. JACS Au, 2021.
27. Khersonsky, O., et al., *Automated design of efficient and functionally diverse enzyme repertoires*. Molecular cell, 2018. **72**(1): p. 178–186. e5.
28. Liu, S., et al., *Novel 3D structure based model for activity prediction and design of antimicrobial peptides*. Scientific reports, 2018. **8**(1): p. 1–12.
29. MacCarthy, E.A., et al., *GPU-I-TASSER: a GPU accelerated I-TASSER protein structure prediction tool*. Bioinformatics, 2022.
30. Zheng, Z.-l., et al., *Construction of a 3D model of nattokinase, a novel fibrinolytic enzyme from Bacillus natto: a novel nucleophilic catalytic mechanism for nattokinase*. Journal of Molecular Graphics and Modelling, 2005. **23**(4): p. 373–380.
31. Chung, I., et al., *Cork-in-bottle mechanism of inhibitor binding to mammalian complex I*. Science Advances, 2021. **7**(20): p. eabg4000.
32. Edachea, E.I., et al., *Docking Simulations and Virtual Screening to find Novel Ligands for T3S in Yersinia pseudotuberculosis YPIII, A drug target for type III secretion (T3S) in the Gram-negative pathogen Yersinia pseudotuberculosis*. Chemical Review and Letters, 2021. **4**(3): p. 130–144.
33. Vora, J., et al., *Structure based virtual screening, 3D-QSAR, molecular dynamics and ADMET studies for selection of natural inhibitors against structural and non-structural targets of Chikungunya*. Journal of Biomolecular Structure and Dynamics, 2019. **37**(12): p. 3150–3161.
34. Loza-Mejía, M.A., J.R. Salazar, and J.F. Sánchez-Tejeda, *In Silico studies on compounds derived from calceolaria: phenylethanoid glycosides as potential multitarget inhibitors for the development of pesticides*. Biomolecules,

2018. **8**(4): p. 121.

35. Agrawal, P., et al., *Benchmarking of different molecular docking methods for protein-peptide docking*. BMC bioinformatics, 2019. **19**(13): p. 105–124.
36. Pitre, L., et al., *New measurement of the Boltzmann constant k by acoustic thermometry of helium-4 gas*. Metrologia, 2017. **54**(6): p. 856.
37. Chen, Z.-S., et al., *Molecular dynamic simulation of the porcine pancreatic lipase in non-aqueous organic solvents*. Frontiers in bioengineering and biotechnology, 2020. **8**: p. 676.
38. Momen, R., et al., *Exploration of the forbidden regions of the Ramachandran plot (ϕ-ψ) with QTAIM*. Physical Chemistry Chemical Physics, 2017. **19**(38): p. 26423–26434.
39. Roy, A.A., et al., *Protein Interaction Z Score Assessment (PIZSA): an empirical scoring scheme for evaluation of protein–protein interactions*. Nucleic acids research, 2019. **47**(W1): p. W331-W337.
40. Yang, J., et al., *Improved protein structure prediction using predicted interresidue orientations.* Proceedings of the National Academy of Sciences, 2020. **117**(3): p. 1496–1503.
41. Zhang, Y. and J. Skolnick, *TM-align: a protein structure alignment algorithm based on the TM-score*. Nucleic acids research, 2005. **33**(7): p. 2302–2309.
42. Kim, D.E., D. Chivian, and D. Baker, *Protein structure prediction and analysis using the Robetta server*. Nucleic acids research, 2004. **32**(suppl_2): p. W526-W531.
43. Park, H., et al., *Automatic structure prediction of oligomeric assemblies using Robetta in CASP12.* Proteins: Structure, Function, and Bioinformatics, 2018. **86**: p. 283–291.
44. Coutsias, E.A., C. Seok, and K.A. Dill, *Using quaternions to calculate RMSD*. Journal of computational chemistry, 2004. **25**(15): p. 1849–1857.
45. Coutsias, E.A. and M.J. Wester, *RMSD and Symmetry*. Journal of computational chemistry, 2019. **40**(15): p. 1496–1508.
46. Jee, A.-Y., T. Tlusty, and S. Granick, *Master curve of boosted diffusion for 10 catalytic enzymes.* Proceedings of the National Academy of Sciences, 2020. **117**(47): p. 29435–29441.
47. Park, J.O., et al., *Metabolite concentrations, fluxes and free energies imply efficient enzyme usage*. Nature chemical biology, 2016. **12**(7): p. 482–489.
48. Musa, A., et al., *Effect of multi-frequency counter-current S type ultrasound pretreatment on the enzymatic hydrolysis of defatted corn germ protein: Kinetics and thermodynamics*. Process Biochemistry, 2019. **87**: p. 112–118.
49. Sudip, R., et al., *Endoglucanase produced by Bacillus subtilis Strain CBS31: Biochemical characterization, thermodynamic study, enzymatic hydrolysis, and bio-industrial applications*. Biotechnology and Bioprocess Engineering: BBE, 2020. **25**(1): p. 104–116.
50. Lapidoth, G., et al., *Highly active enzymes by automated combinatorial backbone assembly and sequence design*. Nature communications, 2018. **9**(1): p. 1–9.
51. Raad, M., et al., *Association of rs2620381 polymorphism in miR-627 and gastric cancer*. British journal of biomedical science, 2020. **77**(2): p. 76–80.
52. Zhang, C., et al., *Blinded testing of function annotation for uPE1 proteins by I-TASSER/COFACTOR pipeline using the 2018–2019 additions to neXtProt and the CAFA3 challenge*. Journal of proteome research, 2019. **18**(12): p. 4154–4166.
53. Zhang, Y., *I-TASSER server for protein 3D structure prediction*. BMC bioinformatics, 2008. **9**(1): p. 1–8.

54. Su, B.-C., et al., *Distribution of positively charged amino acid residues in antimicrobial peptide epinecidin-1 is crucial for in vitro glioblastoma cytotoxicity and its underlying mechanisms*. Chemico-biological interactions, 2020. **315**: p. 108904.
55. Chen, C.R. and G.I. Makhatadze, *Molecular determinant of the effects of hydrostatic pressure on protein folding stability*. Nature communications, 2017. **8**(1): p. 1–9.
56. Rocklin, G.J., et al., *Global analysis of protein folding using massively parallel design, synthesis, and testing*. Science, 2017. **357**(6347): p. 168–175.
57. Tsai, M.Y., et al., *Electrostatics, structure prediction, and the energy landscapes for protein folding and binding*. Protein Science, 2016. **25**(1): p. 255–269.
58. Steinbrecher, T., et al., *Predicting the effect of amino acid single-point mutations on protein stability—large-scale validation of MD-based relative free energy calculations*. Journal of molecular biology, 2017. **429**(7): p. 948–963.
59. Chen, F.F., et al., *Multi-molar absorption of CO2 by the activation of carboxylate groups in amino acid ionic liquids*. Angewandte Chemie, 2016. **128**(25): p. 7282–7286.
60. Mayer-Bacon, C. and S.J. Freeland, *A broader context for understanding amino acid alphabet optimality*. Journal of Theoretical Biology, 2021. **520**: p. 110661.
61. D'Atri, V., et al., *Hydrophilic interaction chromatography hyphenated with mass spectrometry: a powerful analytical tool for the comparison of originator and biosimilar therapeutic monoclonal antibodies at the middle-up level of analysis*. Analytical chemistry, 2017. **89**(3): p. 2086–2092.
62. Zhu, C., et al., *Characterizing hydrophobicity of amino acid side chains in a protein environment via measuring contact angle of a water nanodroplet on planar peptide network.* Proceedings of the National Academy of Sciences, 2016. **113**(46): p. 12946–12951.
63. Riback, J.A., et al., *Response to Comment on "Innovative scattering analysis shows that hydrophobic disordered proteins are expanded in water"*. Science, 2018. **361**(6405).
64. Riback, J.A., et al., *Innovative scattering analysis shows that hydrophobic disordered proteins are expanded in water*. Science, 2017. **358**(6360): p. 238–241.
65. Xi, E., et al., *Hydrophobicity of proteins and nanostructured solutes is governed by topographical and chemical context.* Proceedings of the National Academy of Sciences, 2017. **114**(51): p. 13345–13350.
66. Bergfreund, J., P. Bertsch, and P. Fischer, *Adsorption of proteins to fluid interfaces: Role of the hydrophobic subphase*. Journal of Colloid and Interface Science, 2021. **584**: p. 411–417.
67. Gharibzahedi, S.M.T. and B. Smith, *Legume proteins are smart carriers to encapsulate hydrophilic and hydrophobic bioactive compounds and probiotic bacteria: A review*. Comprehensive Reviews in Food Science and Food Safety, 2021. **20**(2): p. 1250–1279.
68. Pantsar, T. and A. Poso, *Binding affinity via docking: fact and fiction*. Molecules, 2018. **23**(8): p. 1899.
69. Chen, D., et al., *Regulation of protein-ligand binding affinity by hydrogen bond pairing*. Science advances, 2016. **2**(3): p. e1501240.
70. Nivedha, A.K., et al., *Vina-Carb: improving glycosidic angles during carbohydrate docking*. Journal of chemical theory and computation, 2016. **12**(2): p. 892–901.
71. Kim, I.J., H.J. Youn, and K.H. Kim, *Synergism of an auxiliary activity 9 (AA9) from Chaetomium globosum with xylanase on the hydrolysis of xylan and lignocellulose*. Process Biochemistry, 2016. **51**(10): p. 1445–1451.
72. Álvarez-Cervantes, J., et al., *Phylogenetic analysis of β-xylanase SRXL1 of Sporisorium reilianum and its relationship with families (GH10 and GH11) of Ascomycetes and Basidiomycetes*. Scientific reports, 2016. **6**(1): p. 1–9.

73. Li, Q., et al., *Engineering a xylanase from Streptomyce rochei L10904 by mutation to improve its catalytic characteristics*. International journal of biological macromolecules, 2017. **101**: p. 366–372.
74. Sha, C., et al., *Efficient xylan-to-sugar biotransformation using an engineered xylanase in hyperthermic environment*. International journal of biological macromolecules, 2020. **157**: p. 17–23.

Figures

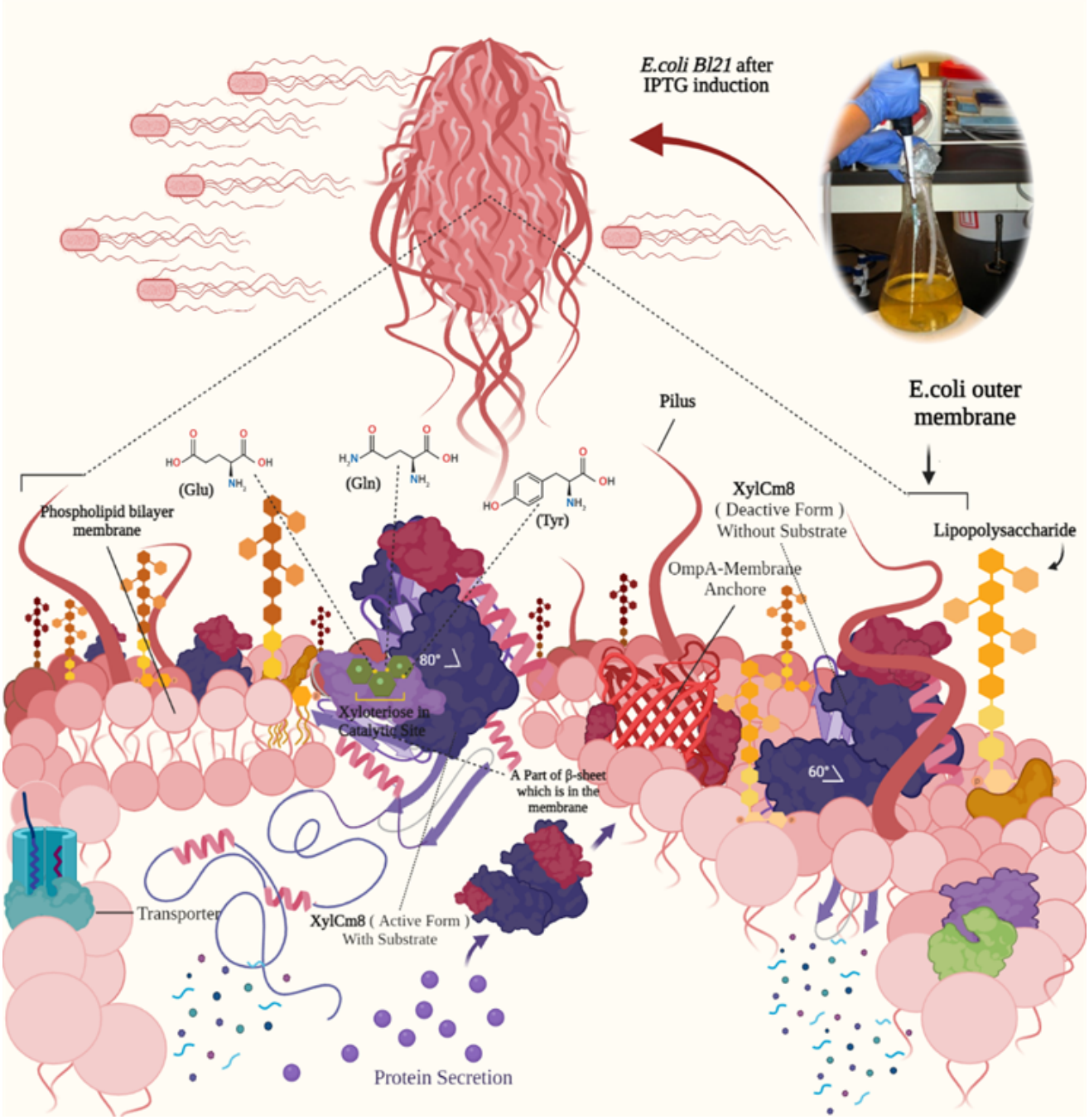


Figure 1

Schematic enzyme position in the outer membrane. XylCm8, its - sheet form (2 - sheets, parallel strand forms with a loop), is located in the membrane. A very little amount of this enzyme can act freely in the cytoplasm and degrade substrates.

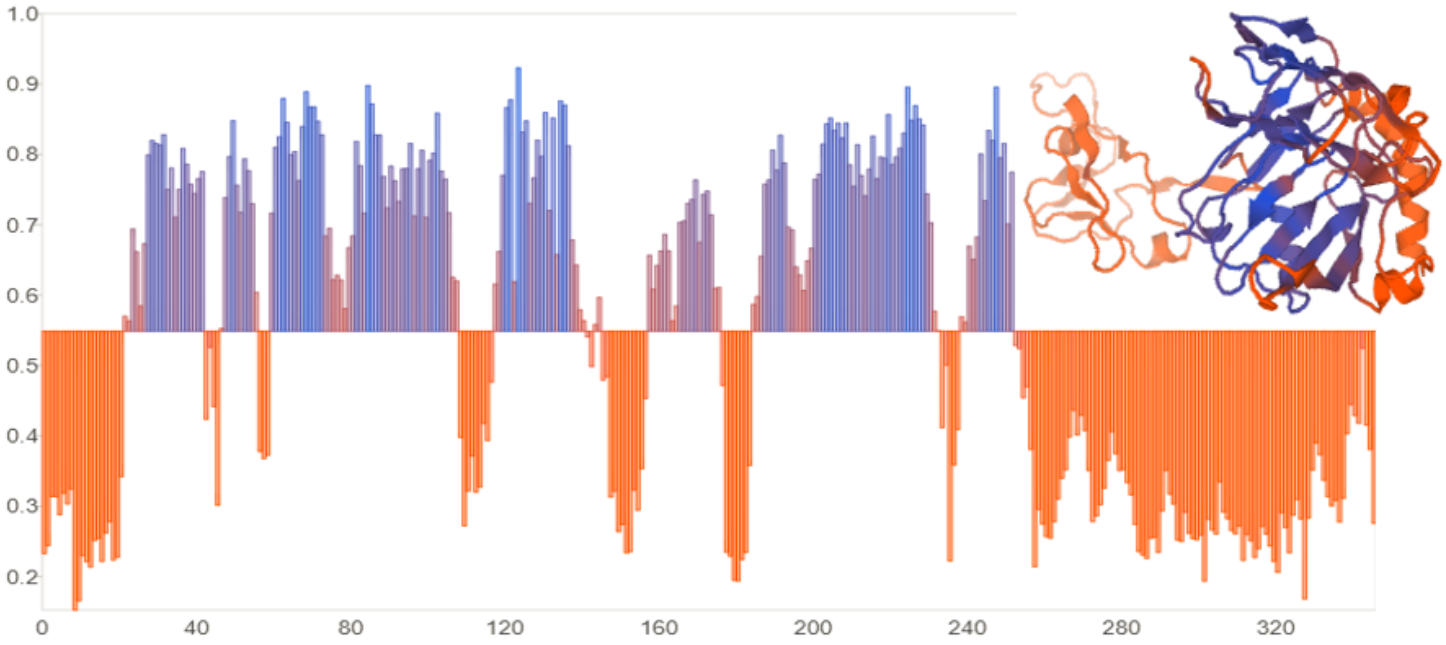


Figure 2

Xylanase structure with QmeanDisco analysis by Swiss Model.

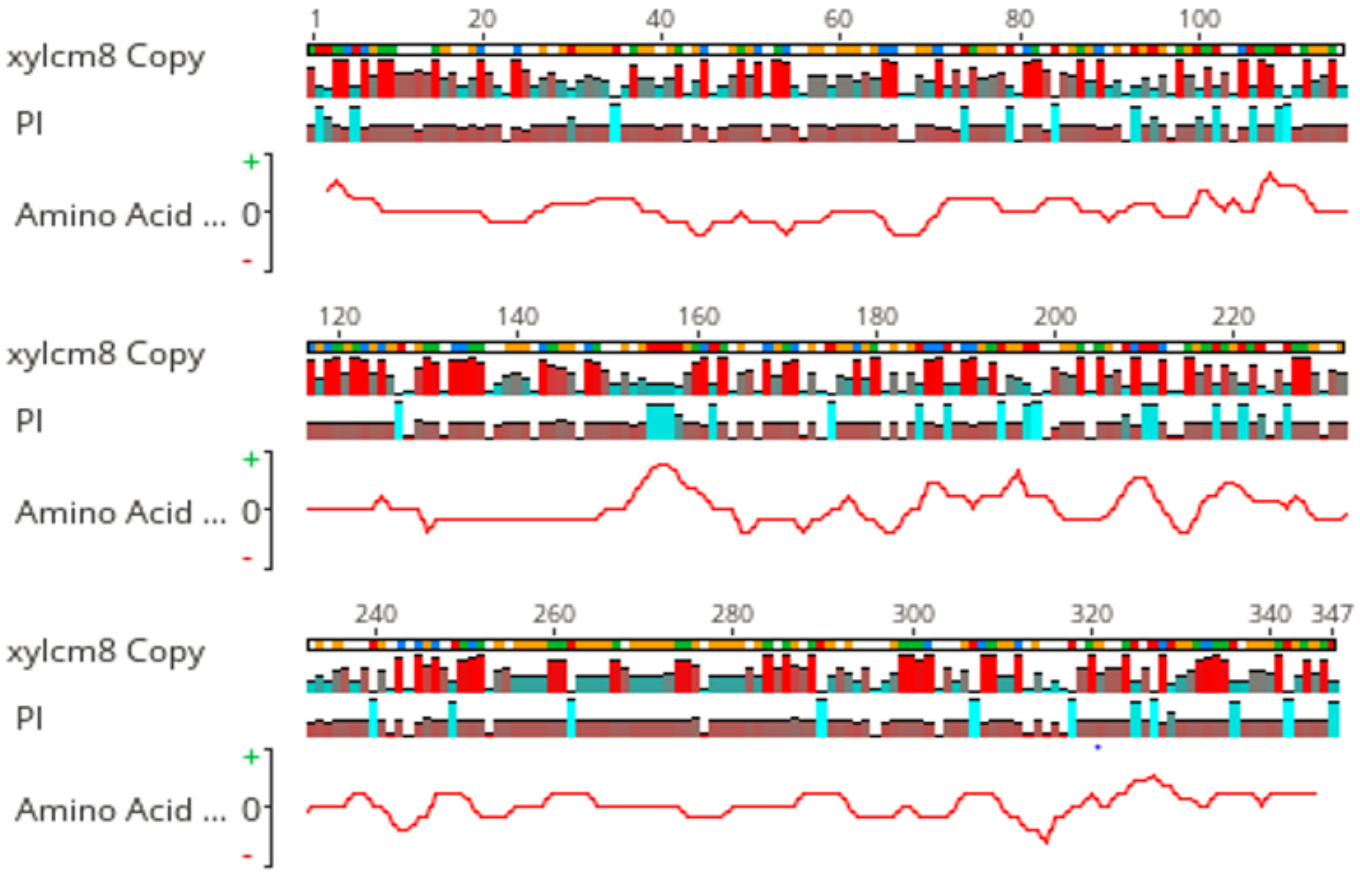


Figure 3

Structural map of the XylCm8, hydrophobicity, PI and amino acid charge. This indicates the enzymatic charge, which is a little in negative form about 5.4%. All these results obtained by Geneious Prime and JalView softwares.

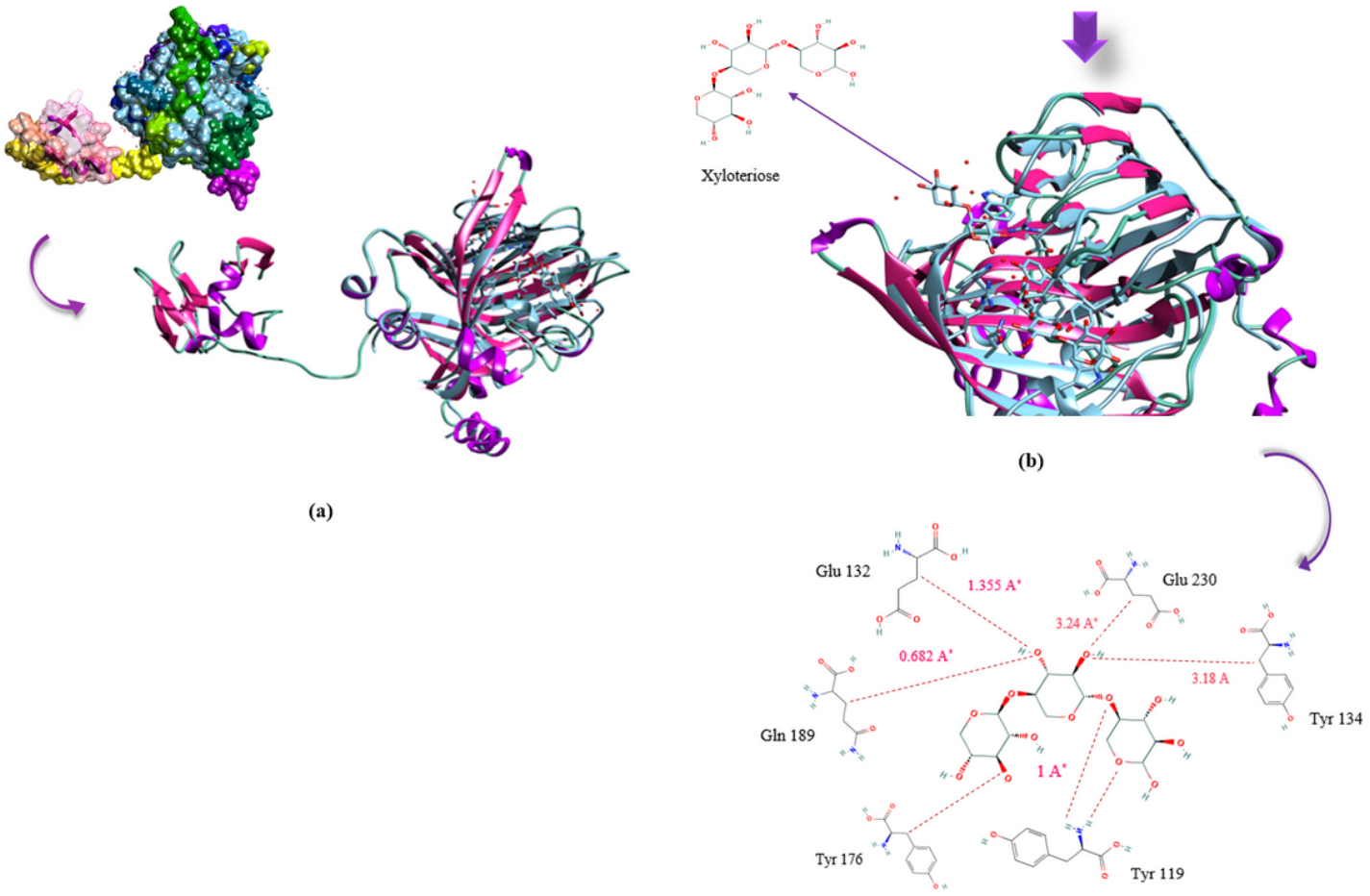


Figure 6

Docking and structural alignment results. Form (**a**) is the Structural alignment with 3WP6 by specific substrate, xyloteriose by Chimera software and (**b**) is Catalytic site and amino acid interactions (Docking) with xyloteriose.



Figure 9

The enzyme mutated sections analyses. Form (**a, b, c)** are mutated sections molecular view of the structure of Xylcm8 by ChimeraX. Form (**b**) shows the amino acid substitution with Arg in two different positions and (**c**) indicates distances between these two substitutions with other close amino acids.

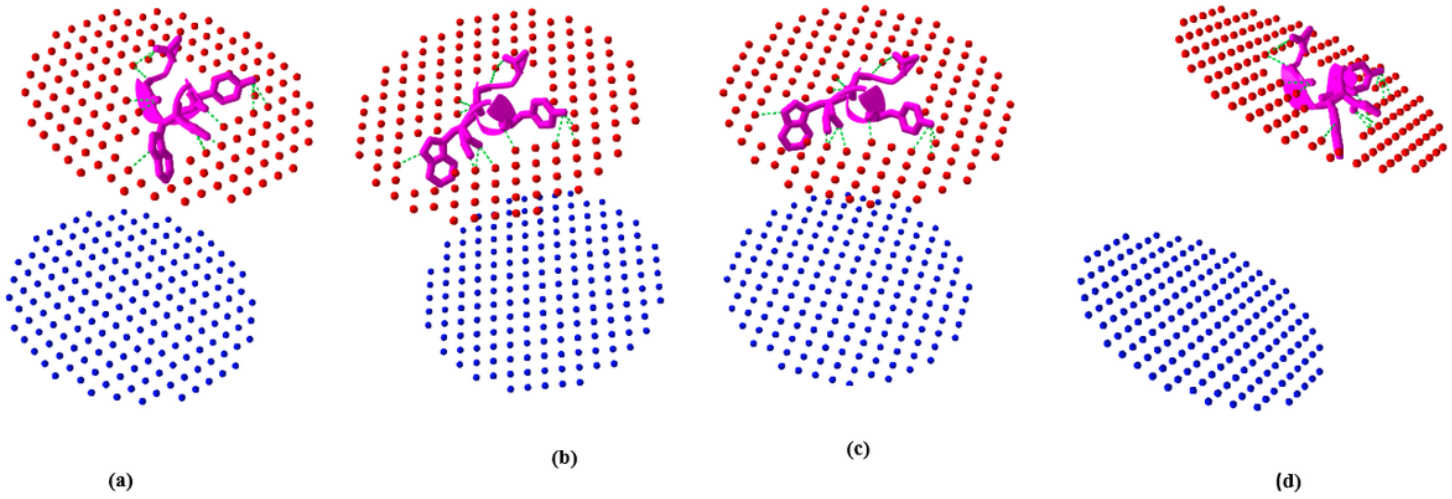


Figure 11

Different α helices positions of mutated and native forms of XylCm8 in the outer membrane by NCBI database and membranome webserver. Forms (**a**, **b**, **c**, and **d**) are some predicted α helices membrane positions which demonstrated with their lateral interactions by the membrane.

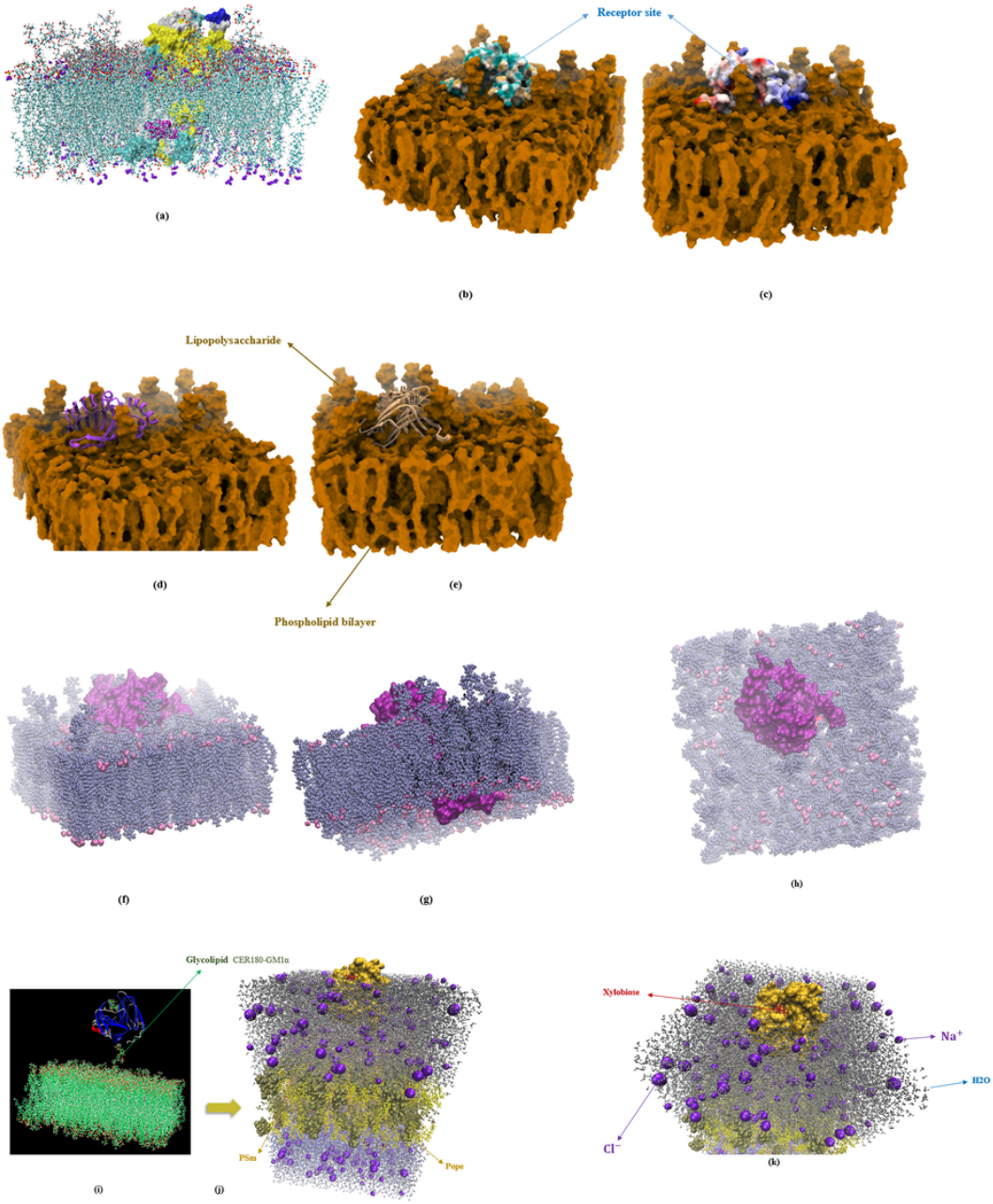


Figure 13

Simulated form of two enzymes in the outer membrane. (**a**-**h**) simulation forms of XylCm8 and the most similar enzyme with it, 3WP6 in forms (**i**, **j** and **k**) and their simulated position in the outer membrane.